

# Reliability of Uptake Estimates in FDG PET as a Function of Acquisition and Processing Protocols Using the CPET

Juliette Feuardent, Marine Soret, Olivier de Dreuille, Hervé Foehrenbach, and Irène Buvat

**Abstract**—Standardized uptake values (SUV) are commonly used in FDG PET to characterize suspicious high uptakes. To better understand the reliability and the limits of SUV, we studied the accuracy of uptake estimates as a function of a number of parameters using phantom data acquired on the CPET. **Methods:** Using the Data Spectrum thorax phantom in which spheres were inserted, we studied the effect of the sphere sizes, of out-of-the-field-of-view activity (OFOVA), of the emission scan duration and of attenuation and partial volume effect (PVE) corrections upon biases in tumor-to-normal tissue uptake ratio (TNR) estimates. Considering a specific acquisition and processing protocol as a reference, we determined the changes in TNR when modifying this protocol. **Results:** For a true TNR of 8, estimated TNR were strongly dependent on lesion size, but also on the acquisition and processing protocol. Depending on the method used to derive the attenuation map, estimated TNR could change by more than 50% for lung spheres less than 2 cm in diameter. Using PVE correction, TNR increased by a factor greater than 2 for spheres less than 2 cm in diameter. The very method used to estimate sphere activity from the reconstructed images could also change the TNR by more than 50%. Even with CT-based attenuation correction and PVE correction, TNR estimates remained underestimated by more than 20% in lesions less than 2 cm in diameter. **Conclusion:** Biases in uptake estimates strongly depend on the acquisition and processing protocols. This suggests that comparing SUV between studies make sense only if the scanner and the acquisition and processing protocols are strictly identical.

**Index Terms**—PET, quantification, standardized uptake values.

## I. INTRODUCTION

STANDARDIZED UPTAKE VALUES (SUV) are commonly used in FDG PET to characterize suspicious high uptakes [1], [2]. However, SUV estimates are biased by a number of phenomena, making their interpretation potentially misleading. The influence of specific phenomena, e.g., the way attenuation correction is performed [3], upon SUV estimates has already been studied. However, how errors of various origins combine still need investigation. We started a detailed investigation of the biases affecting uptake estimates using

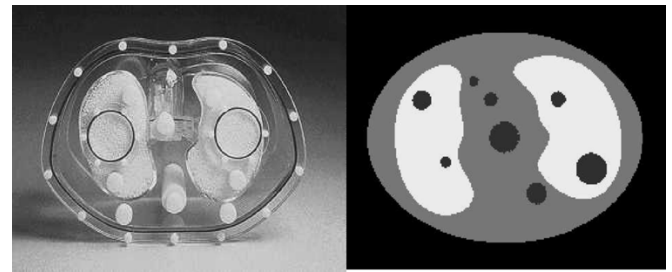


Fig. 1. Data Spectrum thorax phantom and location of the spheres inserted in the phantom.

numerical simulations [4], by considering the effects of lesion size, uptake heterogeneity within the lesion, tumor-to-background activity ratio, attenuation, spatial resolution, tumor location and image sampling. The purpose of the present work was to further investigate the reliability of uptake estimates using real phantom experiments acquired on the CPET. We investigated the effect of two phantom parameters [lesion sizes and out-of-the-field-of-view activity— (OFOVA)], of an acquisition parameter (emission scan duration) and of two processing parameters [attenuation and partial volume effect (PVE) corrections]. We also compared two methods of uptake measurements. Acquisition and processing protocols that minimize the errors in SUV estimates are suggested.

## II. MATERIAL AND METHODS

**Phantom:** A thorax phantom (Data Spectrum Corporation, Hillsborough, NC) including lungs and soft tissues was considered (Fig. 1).

Two identical sets of four spheres, with inner diameters of 10.5, 16, 22, and 33 mm, were introduced in the lung and mediastinum compartments. FDG activity concentrations were set to 30.4 kBq/mL in the spheres and 3.8 kBq/mL in the mediastinum while no activity was introduced in the lungs (cf. Table I). We characterized the accuracy of uptake measurement using the “tumor-to-normal tissue” uptake ratios (TNR) between the spheres and the mediastinum (theoretical value was 8). The percent biases affecting such uptake ratios are actually theoretically identical to those affecting SUV [4].

The impact of OFOVA was studied by adding two activity sources on both sides of the thorax phantom: one water cylinder (19 cm long, 20 cm in diameter) with an FDG activity concentration of 7.4 kBq/mL, and a 500-mL perfusion bag (17 cm long in the axial direction of the tomograph, 10 cm wide, and 2.5

Manuscript received November 16, 2003; revised November 30, 2004.

J. Feuardent and I. Buvat are with the UMR 678 INSERM-UPMC, CHU Pitie Salpetriere, 75634 Paris Cedex 13 France (e-mail: feuardent@imed.jussieu.fr; buvat@imed.jussieu.fr).

M. Soret is with the UMR 678 INSERM-UPMC, CHU Pitie Salpetriere, 75634 Paris Cedex 13 France, and also with the H.I.A. Val-de-Grâce, Paris, France.

O. de Dreuille is with Siemens, Saint-Denis, France.

H. Foehrenbach is with the H.I.A. Val-de-Grâce, Paris, France.

Digital Object Identifier 10.1109/TNS.2005.858222

TABLE I  
ACTIVITY DISTRIBUTION IN THE THORAX PHANTOM AND ASSOCIATED TNR

	Activity concentration (kBq/mL)	Theoretical TNR
Spheres	30.4	8
Soft tissues	3.8	1
Lungs	0.0	0

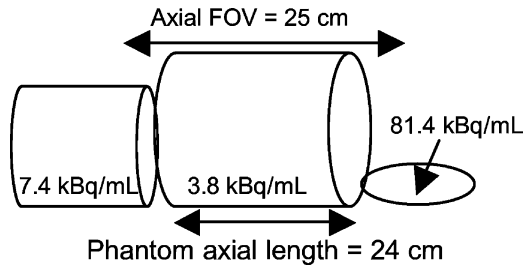


Fig. 2. Activity concentrations in the Data Spectrum thorax phantom and in the out-of-the-field-of-view sources.

cm high) with an FDG activity concentration of 81.4 kBq/mL (Fig. 2).

**PET Acquisitions:** Three-dimensional (3-D) mode emission acquisitions were performed using the CPET tomograph (ADAC-UGM/Philips, Philadelphia, PA). A  $2.25 \times 3 \times 4$  mm spatial sampling was used when acquiring the sinograms. The single count rate was around  $4.10^6$  cps, similar to the count rates observed in clinical acquisitions with the CPET. The impact of the emission acquisition duration on TNR estimates was studied by considering 6- and 18-min emission scan, respectively. The 6-min duration is the default value specified by the manufacturer in the predefined acquisition protocols and the performance of the CPET have already been characterized for this acquisition duration [5]. The 18-min emission scans were obtained by summing three consecutive 6 min emission scans. The CPET corrects the sinograms for “background,” supposedly including randoms and scatter. Background within the object is estimated by fitting the count profiles detected outside the borders of the object (derived from the transmission map) with a parabolic function [6].

To perform attenuation correction, a 2-min transmission scan was also acquired one day after the emission scan, with the  $^{137}\text{Cs}$  transmission point source of the CPET system. The phantom was not moved between the emission and the transmission scans.

**CT Acquisition:** A CT acquisition of the phantom was performed using the Lightspeed scanner (General Electric Medical Systems, Milwaukee, WI). The spatial sampling of the CT data was  $1.56 \text{ mm} \times 1.56 \text{ mm} \times 1 \text{ mm}$ , where 1 mm corresponded to the axial sampling.

#### Data Processing:

**a) Attenuation correction:** The emission sinograms were corrected for attenuation by multiplication with attenuation correction factors (ACF) derived from three different attenuation maps. A so-called Cs map was obtained after “remapping” the  $^{137}\text{Cs}$  transmission scan [8]. This “remapping” considers the histogram of the  $\mu$  values obtained from the transmission scan. To deal with scatter in the transmission data, the histogram is

first shifted so that the value corresponding to its maximum coincides with the  $\mu$  value of water ( $\mu = 0.096 \text{ cm}^{-1}$ ). Theoretical 511-keV attenuation coefficient for soft tissues ( $\mu = 0.096 \text{ cm}^{-1}$ ) is then assigned to the soft tissue compartment pixels, identified as those pixels with  $\mu \leq 0.078 \text{ cm}^{-1}$ . Attenuation coefficients are left unchanged in pixels located in the lungs, identified as those pixels with  $\mu \leq 0.048 \text{ cm}^{-1}$ . Pixels with  $0.048 \text{ cm}^{-1} < \mu < 0.078 \text{ cm}^{-1}$  are given  $\mu$  values obtained by linear interpolation [8]. To perform CT-based attenuation corrections, the CT images were first realigned with the PET images reconstructed without attenuation correction at the CT image sampling ( $1.56 \times 1.56 \times 1 \text{ mm}$ ), using a mutual information maximization algorithm [9]. A so-called S-CT map was then obtained by assigning theoretical 511-keV attenuation coefficients to the lung compartment ( $\mu = 0.035 \text{ cm}^{-1}$ ) and to the soft tissues and sphere compartments ( $\mu = 0.096 \text{ cm}^{-1}$ ) as identified on the CT by manually delineating the contours of 11 compartments: 1 for each of the 8 spheres, 1 for the lungs, 1 for the soft tissues, and 1 for the region outside the phantom. A so-called R-CT map was also obtained as follows: the lung and soft tissues compartments manually segmented were combined with 8 sphere compartments whose volumes were set to be identical to the known sphere volumes, and which were automatically located on the spheres seen on the emission image, by maximizing the signal intensity falling within the spheres. The resulting S-CT and R-CT maps were blurred with a 3-D Gaussian filter to match the spatial resolution of the emission data, namely 12 mm.

**b) Reconstruction:** Attenuation corrected sinograms were reconstructed using ordered subset expectation maximization (OSEM) with eight subsets and six iterations after Fourier rebinning [7], using a homemade reconstruction software. The sampling of the reconstructed PET images was that of the CT, namely  $1.56 \text{ mm} \times 1.56 \text{ mm} \times 1 \text{ mm}$ . Because spatial resolution in the reconstructed images is an input parameter for partial volume effect correction (see Section III), spatial resolution was visually assessed by comparing the reconstructed images with numerically simulated images of the phantom filtered with 3-D Gaussian functions of FWHM varying between 8 and 14 mm. The estimated spatial resolution was 12 mm. Visual analysis of count profiles drawn through the spheres, as illustrated in Fig. 3, confirmed the relevance of the 12-mm spatial resolution estimate.

**c) PVE Correction:** A PVE correction was implemented, requiring the definition of a volume of interest (VOI) corresponding to each sphere. Two VOI sets were considered: one corresponding to the sphere manually segmented on the CT for attenuation correction (set S), the other one corresponding to the spheres with exact volumes used to create the R-CT map (set R). The PVE correction method consisted in multiplying the activity measured in each sphere VOI by an appropriate recovery coefficient (RC). The RCs were estimated using the size of the spheres as estimated from the considered VOI set (underestimated sizes for set S and exact sizes for set R), and considering a 12-mm spatial resolution in the reconstructed images.

**TNR Measurements:** Two TNR indexes, TNRavg and TNRmax, were calculated by considering the mean and maximum values in the sphere VOIs. The VOIs from set S and from

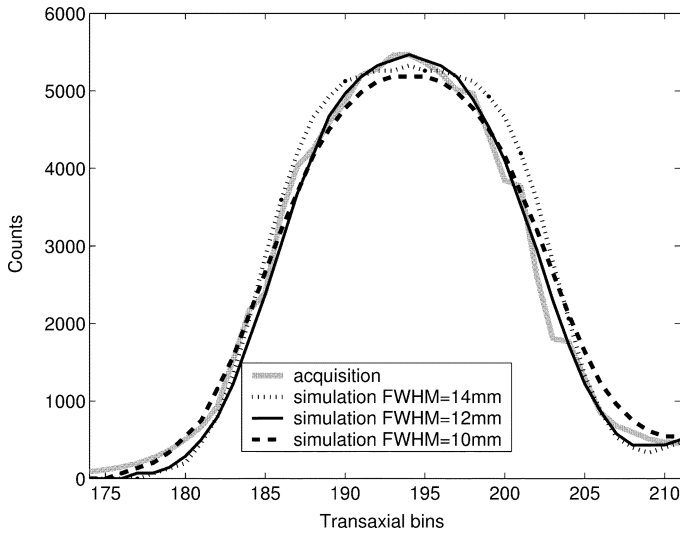


Fig. 3. Visual estimation of the spatial resolution in the reconstructed image: profiles drawn through the 33-mm lung sphere.

set R were systematically considered. The VOI used to estimate the normal value was defined in a soft tissue region chosen to be large enough (including about 80 000 voxels) to have sufficient statistics and far enough from other compartment boundaries not to be affected by PVE. For both TNRavg or TNRmax, the “normal” uptake value was the mean value in the “normal” VOI.

*Data Analysis:* We defined a “reference” configuration, corresponding to no OFOVA, 6 min emission scan, use of the Cs map for attenuation correction, no PVE correction, and calculation of TNRavg. We then studied how the TNR estimates changed when increasing the emission scan duration, when OFOVA was present, when using a CT map instead of the Cs map for attenuation correction, when PVE was corrected for, and when TNRmax was considered instead of TNRavg. Changes in TNR estimates as a function of the imaging and processing protocol and biases in TNR were systematically investigated.

### III. RESULTS AND DISCUSSION

#### A. True Values Considering the Sampling Effect

For small spheres, spatial sampling itself is a source of PVE. Indeed, the true activity distribution is always seen as sampled on the pixel grid. Because of this sampling, the sphere TNR expected from the VOIs corresponding to the R set located in the reconstructed images were below the theoretical value of 8, and varied between 4.8 for the smallest sphere to 6.9 for the largest sphere (Table II). All TNR biases were thus computed with respect to these “sampled” values as follows:  $100 \times (\text{TNR} - \text{sampled TNR}) / \text{sampled TNR}$ .

#### B. Reference Configuration

TNR corresponding to the reference configuration are given in Tables III and IV for the lung spheres and the mediastinal spheres, respectively.

TABLE II  
TRUE TNR CONSIDERING THE SAMPLING EFFECT

	$\phi$ in mm			
	10.5	16	22	33
True TNR (sampling)	4.8	5.8	6.4	6.9

TABLE III  
TNR AND TNR UNDERESTIMATION IN THE “REFERENCE” CONFIGURATION FOR THE LUNG SPHERES

	Spheres in the lungs ( $\phi$ in mm)			
	10.5	16	22	33
TNRavg	0.5	1.4	2.4	3.5
Biases (%)	-90	-76	-63	-49

TABLE IV  
TNR AND TNR UNDERESTIMATION IN THE “REFERENCE” CONFIGURATION FOR THE MEDIASTINAL SPHERES

	Spheres in the mediastinum ( $\phi$ in mm)			
	10.5	16	22	33
TNRavg	1.1	2.0	3.3	4.4
Biases (%)	-77	-66	-48	-36

Results were consistent with previous results obtained using numerical simulations: the smaller the sphere, the greater the TNR underestimation (49% and 90%, respectively, for the largest and the smallest spheres in the lung). TNR were systematically less underestimated for mediastinal spheres than for lung spheres. This is because for the lung spheres, PVE affected the Cs transmission measurement as the spheres had a density different from that of the surrounding lung tissue [4]. As a result, attenuation in the lung spheres was underestimated and attenuation correction did not restore enough counts. Because the mediastinal spheres had a density similar to that of the surrounding soft tissues compartment, PVE did not affect the Cs transmission measurements much, and attenuation was more accurately compensated for compared to the lung spheres. The TNR in the smallest lung sphere was smaller than 1 because there was no activity in the lung. Therefore, the large spill-out reducing the activity in the sphere was not compensated by any spill-in and the sphere activity was smaller than the mediastinal activity.

#### C. Changes in TNR Estimates as a Function of the Imaging and Processing Protocols

*OFOVA:* TNR tended to be greater with OFOVA than without (Tables V, VI, VII, and VIII). Although the considered OFOVA was somehow an extreme case (located at both ends of a rather short cylinder with activity concentrations higher than in the background activity of the cylinder of interest), the changes in TNR were never greater than 10%. The small impact of OFOVA can be explained by the systematic “background” subtraction applied to all acquired data, which subtracted both randoms and scatter on the CPET. Our observations suggest that this correction is not ideal, since there is still an impact of

TABLE V  
CHANGES IN TNR WITH RESPECT TO TNR<sub>REF</sub>, DEFINED BY  $100(TNR - TNR_{REF})/TNR_{REF}$  FOR THE LUNG SPHERES

Changes with respect to the reference values (%)	Spheres in the lungs (Ø in mm)			
	10.5	16	22	33
With OFOVA	6	1	2	5
18 min emission scan	-7	7	2	6
CT attenuation correction	48	46	16	6
PVE correction	999	289	122	60
TNR <sub>max</sub>	37	66	71	81

TABLE VI  
CHANGES IN TNR WITH RESPECT TO TNR<sub>REF</sub>, DEFINED BY  $100(TNR - TNR_{REF})/TNR_{REF}$  FOR THE MEDIASTINAL SPHERES

Changes with respect to the reference values (%)	Spheres in the mediastinum (Ø in mm)			
	10.5	16	22	33
With OFOVA	-10	8	1	4
18 min emission scan	8	1	0	3
CT attenuation correction	3	2	-4	4
PVE correction	105	144	85	46
TNR <sub>max</sub>	33	50	47	50

TABLE VII  
TNR BIASES WITH RESPECT TO SAMPLED TNR, DEFINED BY  $100(TNR - \text{sampledTNR})/\text{sampledTNR}$  FOR THE LUNG SPHERES

TNR biases in %	Spheres in the lungs (Ø in mm)			
	10.5	16	22	33
With OFOVA	-90	-76	-62	-47
18 min emission scan	-91	-75	-62	-47
CT attenuation correction	-86	-65	-56	-47
PVE correction	8	-6	-16	-20
TNR <sub>max</sub>	-87	-60	-36	-9

TABLE VIII  
TNR BIASES WITH RESPECT TO SAMPLED TNR, DEFINED BY  $100(TNR - \text{sampledTNR})/\text{sampledTNR}$  FOR THE MEDIASTINAL SPHERES

TNR biases in %	Spheres in the mediastinum (Ø in mm)			
	10.5	16	22	33
With OFOVA	-79	-63	-48	34
18 min emission scan	-75	-65	-49	-35
CT attenuation correction	-76	-65	-51	-34
PVE correction	-52	-16	-5	-8
TNR <sub>max</sub>	-69	-49	-25	-5

OFOVA, but that it is quite effective at removing most of the signal coming from OFOVA.

*Duration of the Emission Acquisition:* Lengthening the emission acquisition from 6 to 18 min did not affect the TNR much: changes in TNR were never greater than 8% (Tables V, VI, VII and VIII). These results are consistent with previously reported results [10] in which the bias on the SUV decreased by less than 15% when the emission scan duration changed from 15 to 5 min. Indeed, the scan duration mostly changes the noise level in the data, while  $TNR_{avg}$  is not very sensitive to noise—unlike  $TNR_{max}$ —as it is calculated from the average of signal in the VOIs. The noise level (measured as the ratio between the standard deviation and the mean in a VOI drawn over a region with supposedly uniform activity) was around

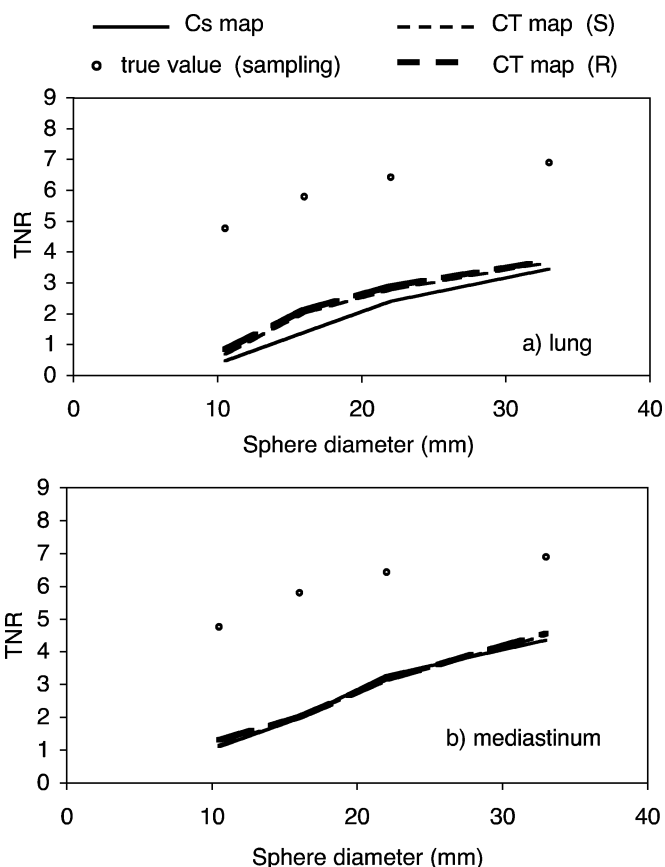


Fig. 4. (a) Measured TNR in the lung spheres. (b) In the mediastinal spheres using the CT (with R and S sphere volumes) or Cs map for attenuation correction.

1.8 times greater in the 6-min emission scan than in the 18-min emission scan. Considering the reference configuration but the 18-min emission scan and  $TNR_{max}$ ,  $TNR_{max}$  increased by 18%, 12%, 14%, and 7%, respectively, for the smallest to the largest lung spheres, when increasing the emission scan duration from 6 to 18 min. For the smallest to the largest mediastinal spheres,  $TNR_{max}$  increased by 14%, 15%, 13%, and decreased by 1%, respectively.

*Attenuation Map:* The type of attenuation map affected the TNR only for the lung spheres, with TNR systematically higher (hence, TNR biases systematically smaller) when the CT maps (either the R-CT or the S-CT map) were used instead of the Cs map (Tables V, VI, VII, and VIII, and Fig. 4). The smaller the sphere diameter, the greater the impact of the attenuation map. Because of the limited spatial resolution of the Cs map, PVE affected the Cs transmission measurements. PVE in transmission yielded an underestimation of the attenuation coefficients in the spheres located in the lungs, as counts transmitted through the lung tissues were detected at the sphere locations (Table IX). Therefore, attenuation was undercorrected in the lung spheres. This effect was also present when using the CT maps (both for the R- and S-CT maps) due to the postfiltering of the segmented acquisition, but was less severe than for the Cs map. The TNR were therefore less underestimated when using the CT maps for attenuation correction than when using the Cs map. The changes in uptake estimates observed in the lung spheres as a function of

TABLE IX  
PERCENT ERRORS IN ATTENUATION COEFFICIENTS ( $\mu$ ) DEFINED BY  $[100(\text{estimated } \mu - \text{theoretical } \mu)/\text{theoretical } \mu]$  FOR THE LUNG AND MEDIASTINAL SPHERES

Errors in %		$\varnothing$ in mm			
		10.5	16	22	33
Cs	Lung spheres	-79	-80	-50	-32
map	Mediastinal spheres	0	0	0	0
S-CT	Lung spheres	-59	-48	-36	-25
map	Mediastinal spheres	0	0	0	0
R-CT	Lung spheres	-52	-41	-32	-22
map	Mediastinal spheres	0	0	0	0

the attenuation map tended to be greater (between 6% and 48%) than those previously reported in a phantom study (between 3% and 15% [3]) and in a patient study (between 4.3% and 15.2% [11]). This might be because the difference in spatial resolution of the two attenuation maps we considered (around 12 mm for the CT maps and more than 16 mm for the Cs map) was greater than the difference in spatial resolution of the two attenuation maps considered in these other studies.

The type of attenuation map (CT or Cs) did not affect TNR estimates in the mediastinal spheres. Indeed, attenuation in these spheres was similar to that of the surrounding water compartment so that the spheres and surrounding medium were not differentiated in the transmission scan, had it been performed with the Cs source or with the CT.

**PVE Correction:** Without PVE correction, the TNR underestimation was between 36% (largest mediastinal sphere) and 90% (smallest lung sphere) in the reference configuration (Tables III and IV). PVE correction strongly increased the TNR, by a factor greater than two for spheres less than 2 cm in diameter (percent changes >100% in Tables V and VI, see also Tables VII and VIII and Fig. 5). This is consistent with the fact that PVE strongly affect measurements in structures less than two to three times the spatial resolution in the reconstructed images [12], [13], i.e., less than 24 to 36 mm in diameter in our case. After PVE correction, TNR were still biased by 8%, -6%, -16%, and -20% from the smallest to the largest lung spheres. In the mediastinal spheres, TNR were biased by -52%, -16%, -5%, and -8% after PVE correction.

Even if PVE correction greatly reduced the bias in TNR estimates, TNR were estimated with a bias less than 20% only for spheres greater than 22 mm in diameter. For spheres <22 mm in diameter, some TNR remained largely biased even when using an optimal protocol including CT attenuation correction and PVE correction (Table X). For the lung spheres, part of the residual biases was due to errors in segmenting the spheres. Indeed, sphere volumes as estimated from the manual segmentation of the CT were all underestimated (Table XI—the smaller the sphere, the greater the volume underestimation) and for spheres <22 mm in diameter, there was a definite impact of the sphere volume upon the TNR estimates (see difference between sets S and R in Table X). These errors in volume estimates from the CT are typical of segmentation errors reported in the literature [14], [15]. The accuracy of the segmentation step, hence, of sphere volume estimates, affect attenuation correction, PVE correction and TNR estimates. When the volume of the structure of interest is underestimated, PVE is corrected too

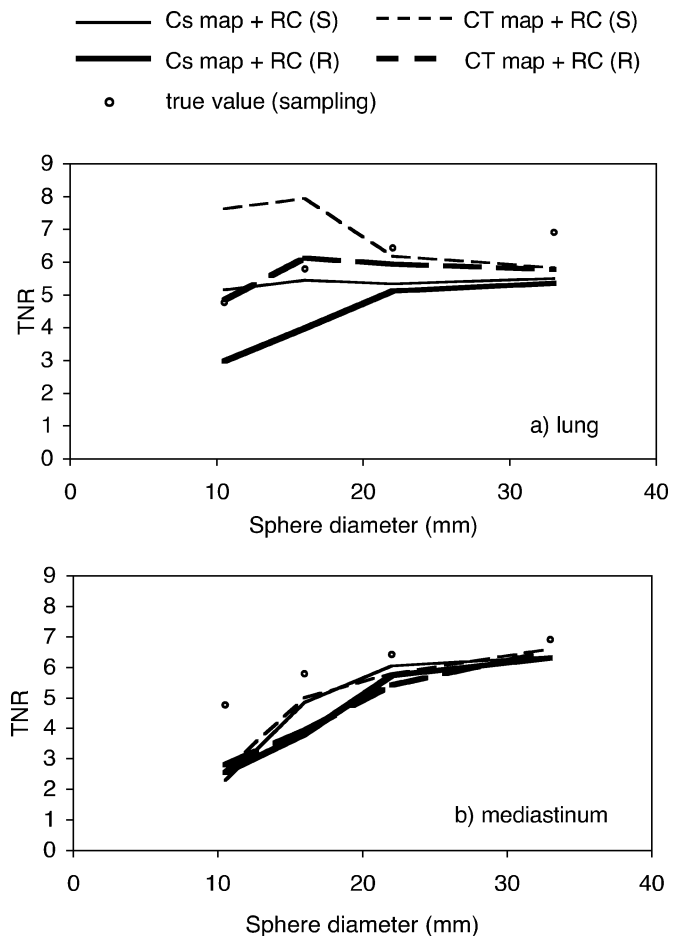


Fig. 5. Measured TNR in the lung spheres (a) and in the mediastinal spheres (b) using the CT or Cs map for attenuation correction, and after PVE correction. Results obtained for exact (R) and segmented (S) sphere volumes are shown.

TABLE X  
RESIDUAL BIASES ON TNR ESTIMATED ON DATA PROCESSED WITH AN OPTIMAL PROTOCOL INCLUDING CT-BASED ATTENUATION AND PVE CORRECTION, CONSIDERING SEGMENTED (S) OR EXACT (R) VOI

TNR residual biases in %	$\varnothing$ in mm			
	10.5	16	22	33
Lung spheres (S)	59	37	-3	-15
Mediastinal spheres (S)	-45	-14	-9	-4
Lung spheres (R)	1	6	-7	-16
Mediastinal spheres (R)	-41	-32	-15	-5

TABLE XI  
PERCENT ERRORS IN INNER VOLUME ESTIMATES CONSIDERING SEGMENTED VOIS, DEFINED BY  $100(\text{estimated volume} - \text{true volume})/\text{true volume}$  FOR THE LUNG AND MEDIASTINAL SPHERES

Errors in %	$\varnothing$ in mm			
	10.5	16	22	33
Lung spheres	-57	-44	-20	-11
Mediastinal spheres	-57	-37	-18	-12

much, which should lead to TNR overestimation. On the other hand, for the spheres located in the lungs, an underestimation of the sphere volume yields an underestimation of attenuation, as part of the sphere tissue is seen as lung tissue. Insufficient attenuation correction yields TNR underestimation. Finally, the size of the VOI considered to calculate  $TNR_{avg}$  also affects

TNR estimates. If the VOI is too small, TNR is less biased by PVE than if the VOI is too large. The precise way these TNR overestimation and underestimation combine to yield the final bias in TNR is complex. In addition, errors in volume estimates are not the only source of residual biases in TNR as biases are still observed when using the R set. Other sources are approximate attenuation correction, especially for the lung spheres affected by transmission PVE, and inaccurate estimation of the spatial resolution in reconstructed images. Indeed, the PVE correction assumes a stationary spatial resolution in the reconstructed images, while spatial resolution is known to be nonstationary. For the CPET for instance, intrinsic transaxial spatial resolution measured on the sinograms is 4.8 and 6.5 mm at 1 and 10 cm from the center of the FOV [16].

*TNR Index:* By definition, TNR<sub>max</sub> were systematically higher, and usually less biased than TNR<sub>avg</sub>. Although this could suggest that TNR<sub>max</sub> should be preferred to TNR<sub>avg</sub> for accurate TNR estimates, using TNR<sub>max</sub> yields biases that strongly depend on the noise level in the images. For instance, TNR<sub>max</sub> was  $12 \pm 6\%$  higher on average on the 18-min scan compared to the 6-min scan, because of the difference in noise in these two scans, while TNR<sub>avg</sub> differed only by  $3 \pm 5\%$  on average between the 18 min scan and the 6 min scan. In [10], a large variability of TNR<sub>max</sub> was also demonstrated when comparing 15 min and 1 min transmission scan durations.

Overall, differences in TNR estimates greater than 100% (i.e., by a factor greater than 2) were observed only because of differences in the acquisition and processing protocols. This suggests that comparing uptake estimates between studies makes sense only if the acquisitions are performed on the same scanner, under identical conditions, and if processing remains unchanged between repeated acquisitions. A meta-analysis of SUV reported in different papers is currently almost impossible given the variability of the biases affecting SUV as currently assessed in different PET centers. This is all the more true given that many other factors also affect SUV and have not been considered in our study, such as blood glucose level, time between injection and imaging session, reconstruction algorithm, or differences between anatomical and functional contours of the lesion. A preliminary step to deal with the variability of SUV estimates associated with changes in acquisition and processing protocols might be a precise characterization of SUV estimate accuracy and variability obtained at different centers for optimized acquisition and processing protocols. Such characterization should make it possible to systematically associate some quantitative indications regarding the biases and variability potentially affecting the reported SUV estimates.

#### IV. CONCLUSION

Biases in uptake estimates slightly depend on the emission scan duration. Depending on lesion location, they can strongly depend on the attenuation map used for attenuation correction. They also strongly depend on whether PVE is corrected for and on whether uptake is calculated using the average count value within the tumor VOI or using the maximum value at the tumor

location. Differences in TNR estimates greater than 100% (i.e., by a factor greater than 2) can be caused only by differences in the way data are acquired and processed, which suggest that comparison of TNR between PET centers using different scanners, different acquisition protocols or different processing is almost impossible. Even when using CT-based attenuation correction and PVE correction, TNR estimates can still be biased by up to 50% in lesions less than 2 cm in diameter. In addition, because of the multifactorial origin of biases affecting TNR measurements, biases related to small lesions cannot be easily predicted, at least when working on the CPET.

#### REFERENCES

- [1] W. A. Weber, V. Petersen, B. Schmidt, L. Tyndale-Hines, T. Link, C. Peschel, and M. Schwaiger, "Positron emission tomography in non small-cell lung cancer: prediction of response to chemotherapy by quantitative assessment of glucose use," *J. Clin. Oncol.*, vol. 21, pp. 2651–2657, 2003.
- [2] N. Pandit, M. Gonen, L. Krug, and S. M. Larson, "Prognostic value of [18F]FDG-PET imaging in small cell lung cancer," *Eur. J. Nucl. Med. Mol. Imag.*, vol. 30, pp. 78–84, 2003.
- [3] D. Visvikis, D. C. Costa, I. Croasdale, A. H. R. Lonn, J. Bomanji, S. Gacinovic, and P. J. Ell, "CT-based attenuation correction in the calculation of semi-quantitative indices of [<sup>18</sup>F]FDG PET uptake in PET," *Eur. J. Nucl. Med.*, vol. 30, pp. 344–353, 2003.
- [4] M. Soret, C. Riddell, S. Hapdey, and I. Buvat, "Biases affecting the measurements of tumor-to-background activity ratio in PET," *IEEE Trans. Nucl. Sci.*, vol. 25, pp. 2112–2118, 2002.
- [5] L. E. Adam, J. S. Karp, M. E. Daube-Witherspoon, and R. J. Smith, "Performance of a whole-body PET scanner using curve-plate NaI(Tl) detectors," *J. Nucl. Med.*, vol. 42, pp. 1821–1830, 2001.
- [6] J. S. Karp, G. Muehllehner, D. A. Mankoff, C. E. Ordonez, J. M. Ollinger, M. E. Daube-Witherspoon, A. T. Haigh, and D. J. Beerbohm, "Continuous-slice PENN-PET: a positron tomograph with volume imaging capability," *J. Nucl. Med.*, vol. 31, pp. 617–627, 1990.
- [7] M. Defrise, P. E. Kinahan, D. W. Townsend, and C. Michel, "Exact and approximate rebinning algorithms for 3-D PET data," *IEEE Trans. Med. Imag.*, vol. 16, pp. 145–158, 1997.
- [8] F. Benard, R. J. Smith, R. Hustinx, J. S. Karp, and A. Alavi, "Clinical evaluation of processing techniques for attenuation correction with <sup>137</sup>Cesium in whole-body PET images," *J. Nucl. Med.*, vol. 40, pp. 1257–1263, 1999.
- [9] F. Maes, A. Collignon, D. Vandermeulen, G. Marchal, and P. Suetens, "Multimodality image registration by maximization of mutual information," *IEEE Trans. Med. Imag.*, vol. 16, pp. 187–198, 1997.
- [10] D. Visvikis, C. Cheze-Le-Rest, D. C. Costa, J. Bomanji, S. Gacinovic, and P. J. Ell, "Influence of OSEM and segmented attenuation correction in the calculation of standardized uptake values for [<sup>18</sup>F]FDG PET," *Eur. J. Nucl. Med.*, vol. 28, pp. 1326–1335, 2001.
- [11] Y. Nakamoto, M. Osman, C. Cohade, L. T. Marshall, J. M. Links, S. Kohlmyer, and R. Wahl, "PET/CT: comparison of quantitative tracer uptake between germanium and CT transmission attenuation-corrected images," *J. Nucl. Med.*, vol. 43, pp. 1137–1143, 2002.
- [12] E. J. Hoffman, S. C. Huang, and M. E. Phelps, "Quantitation in positron emission computed tomography: 1 effect of object size," *J. Comput. Assist. Tomogr.*, vol. 3, pp. 299–308, 1979.
- [13] R. M. Kessler, J. R. Ellis, and M. Eden, "Analysis of emission tomographic scan data: limitations imposed by resolution and background," *J. Comput. Assist. Tomogr.*, vol. 8, pp. 514–522, 1984.
- [14] S. A. Sohaib, B. Turner, J. A. Hanson, M. Farquarson, R. T. D. Olivier, and R. H. Reznick, "CT assessment of tumour response to treatment: comparison of linear, cross-sectional and volumetric measures of tumour size," *Br. J. Radiol.*, vol. 73, pp. 1178–1184, 2000.
- [15] C. Schiepers, M. Brown, S. Rogers, M. McNitt-Gray, M. E. Phelps, and M. Dahlbom, "Lesion size and volume in combining PET and CT: phantom experiments," *J. Nucl. Med.*, vol. 43, 2002.
- [16] I. Buvat, I. Castiglioni, J. Feuervent, and M. C. Gilardi, "Unified description and validation of Monte Carlo simulators in PET," *Phys. Med. Biol.*, 2005.